Hydrothermal carbonization of sewage sludge: Multi-response optimization of hydrochar production and CO_2-assisted gasification performance

Shuai Guo
Northeast Electric Power University
DanDan Xu
Northeast Electric Power University
Xin Guo
Harbin Boiler Co Ltd
Xingcan Li
Northeast Electric Power University
Chenchen Zhao (490268719@qq.com)
Northeast Electric Power University

Research Article

Keywords: sewage sludge, hydrothermal carbonization, gasification, response surface methodology, waste-to-energy

Posted Date: November 2nd, 2021

DOI: https://doi.org/10.21203/rs.3.rs-954940/v1

Abstract

The harmful effects of improper sewage sludge (SS) treatment on the environment inspire the search for more benign sludge processing techniques such as hydrothermal carbonization (HTC); the abundant organic matter in SS is used for energy recovery. Herein, response surface methodology (RSM) was used to optimize the HTC-based preparation of SS hydrochar and its gasification performance. Specifically, the hydrochar yield, higher heating value (HHV), and gasification activity index were selected as optimization goals, while carbonization temperature (160–260°C), residence time (30–150 min), and acetic acid concentration (0–1.5 M) were selected as factors influencing the HTC process and CO_2-assisted gasification performance. Carbonization temperature was the dominant parameter determining hydrochar yield, HHV, and gasification activity. The hydrochar yield (82.69%) and calorific value (7820.99 kJ kg^{-1}) were maximized under comparatively mild conditions (160°C, 30 min, and 0.07 M acetic acid), whereas the gasification activity index (0.288 s^{-1}) was maximized under harsher conditions (211.34°C, 88.16 min, and 1.58 M acetic acid). The obtained results help to guide the HTC of SS intended for gasification, thus promoting the development of this promising waste-to-energy technology, and may facilitate the design and further optimization of thermochemical SS conversion.

1. Introduction

According to recent estimates, the amount of domestic and industrial wastewater generated worldwide each year is of the order of billions of tons and is expected to increase because of population growth and living standard improvement (Mateo-Sagasta et al. 2015; Bora et al. 2020), which in turn will cause serious pollution (Meng et al. 2016). Compared with the traditional methods of wastewater SS disposal (e.g., landfilling, incineration, and anaerobic digestion), which suffer from land shortage, secondary pollution, and long processing duration, the thermochemical conversion of SS by gasification offers the advantages of decreased pollutant emission and shorter processing duration, thus holding great promise (Zheng et al. 2020; Chen et al. 2020).

However, the gasification-based conversion of SS to valuable energy and fuels is hindered by its high moisture content. Currently, at least 50 million tons of SS with a moisture content of 80% are produced within the European Union annually (Kelessidis et al. 2012), and a similar value (40 million tons of SS with a moisture content of 80%) has been estimated for the United States and China (Venkatesan et al. 2015). Since most of the energy invested and released during the conventional heat treatment process is consumed to remove SS moisture, this has inspired the search for innovative and sustainable SS pre-drying technologies.

The main advantage of Hydrothermal carbonization (HTC) over other thermal conversion technologies, such as pyrolysis, gasification and incineration, is its ability to convert wet sludge to hydrochar with relatively high yields without preliminary dewatering and drying, which, consequently, requires less energy. Therefore, HTC has received much attention as a pretreatment technology allowing the effective conversion of wet biomass into solid fuel (hydrochar) (Yu et al. 2018; He et al. 2018), is a pressurized thermal conversion process that is achieved at a mild temperature (160–300°C) and self-generated pressure for various retention time (Sharma et al. 2020); it involves five principal reactions, namely hydrolysis, dehydration, decarboxylation, polymerization, and aromatization (Zhao et al. 2014; Reza et al. 2014). The feasibility of employing HTC to prepare solid fuel from biomass waste has therefore been extensively investigated (Park et al. 2018; Peng et al. 2016). Park et al. showed that the HTC of algal biomass affords hydrochar with improved carbon content, carbon recovery, energy recovery, and C/O and C/H atomic ratios (Park et al. 2018). Some researchers have observed a significant enhancement in SS dewaterability

after HTC (Peng et al. 2016; Escala et al. 2012; Kim et al. 2014; Wang et al. 2015). He et al. used HTC to convert SS into a clean solid fuel, achieving an 88% carbon recovery while removing 60% of nitrogen and sulfur (He et al. 2013). Atallah et al. found that with increasing reaction time and solid-to-liquid ratio, hydrochar yield decreased from 36 to 7%, while the carbon and energy contents increased to 76% and 36 MJ kg^{-1}, respectively (Atallah et al. 2019). Lee et al. demonstrating that in terms of yield and higher heating value (HHV), the potential of hydrochar as a fuel increased at a relatively low HTC treatment temperature (180–200°C). (Lee et al. 2019). In addition to temperature and residence time, the type of acid catalyst is also an important factor affecting the performance of HTC-produced fuel. Liu et al. showing that acidic conditions favor hydrochar aromatization (Liua et al. 2020). Evcil et al. revealing that acid catalysis can reduce hydrochar yield and HHV and showed that although irregular carbon spheres formed at all temperatures tested in the catalytic runs, no such spheres were produced in non-catalytic runs (Evcil et al. 2020). Given that the acids produced during hydrothermal biomass processing catalyze HTC (Stemann et al. 2013), we herein considered the influence of the most abundant of these acids, namely acetic acid.

Numerous works show that HTC improves the fuel properties of sludge and provides raw materials more suitable for further thermochemical conversion (Park et al. 2018; Peng et al. 2016; Escala et al. 2012; Kim et al. 2014; Wang et al. 2015; He et al. 2013; Atallah et al. 2019; Lee et al. 2019). Gai et al. demonstrating that hydrochar contained more alkali and alkaline earth metals and featured higher gasification reactivity. In addition, the porous structure of hydrochar was claimed to result in higher gas yield and gasification efficiency (Gai et al. 2016). Zheng et al. found that higher hydrothermal reaction times and temperatures reduce H_2 production (Zheng et al. 2019). Lin et al. demonstrating that after HTC the CO_2-assisted gasification of coke could be completed in a quite short time, and the reactivity of hydrochar was found to exceed that of the raw material (Lin et al. 2016). Wei et al. studied the characteristics of CO_2-assisted hydrochar gasification and found that the gasification activity could be enhanced by increasing the gasification temperature and hydrochar mixing ratio (Wei et al. 2017). Moon et al. showing that the amount and HHV of the gas produced by steam gasification increased after the hydrothermal treatment of SS (Moon et al. 2015). Mosqueda et al. probe the CO_2-assisted gasification behaviors of washed and non-washed banana leaf hydrochars, revealing that both hydrochars featured a decreased alkali content and thus had lower gasification reactivities than the raw materials (Mosqueda et al. 2019). Most existing reports on hydrochar gasification mainly employ steam as the gasification agent, whereas the use of CO_2 for sludge hydrochar gasification remains underexplored. Given that the energy consumption as well as the emissions and costs related to the generation of superheated steam are not negligible, CO_2-assisted gasification has attracted much attention, allowing the simultaneous generation of energy and the reduction of overall CO_2 emissions (Parvez et al. 2016). Therefore, in this study, we probed the gasification of SS hydrochar in an atmosphere of CO_2.

The recent years have witnessed a surge of interest in the optimization of HTC conditions using the response surface methodology (RSM). A response surface model describing the relationship between the given factors and the response values is constructed by using appropriate functions, and the optimal process parameters are obtained by analyzing these relationships and dealing with multivariable problems (Franceschini et al. 2008). Oluwasola et al. used RSM to maximized the yield and HHV of hydrochar produced from coffee grounds. Under the optimal reaction conditions of 216°C and 1 h, the maximal hydrochar yield and HHV equaled 64% and 31.6 MJ kg^{-1}, respectively (Afolabi et al. 2020). Kang et al. used RSM to optimize the microwave-assisted HTC of corn stalks. Statistical analysis showed that temperature is the main factor governing product quality and HHV. Under the optimal conditions of 181.9°C, 39.7 min, and 3.8 g/50 mL H_2O, the yield achieved 80.55%. Under the conditions of 230°C, 45 min, and 2 g/50 mL H_2O, the HHV equaled 22.82 MJ kg^{-1}, exceeding the value of raw corn stalks by

41% (Kang et al. 2019). These results indicate that RSM is a well-established and widely used technique for studying the joint interactions between independent (input) variables in the reaction process and is particularly useful for process optimization.

Despite the great potential of HTC and subsequent hydrochar gasification, information on statistically optimized conditions for realizing best-quality hydrochar for energy applications is still scarce. Herein, RSM is used to establish the optimal HTC conditions for maximizing hydrochar yield and HHV as well as to determine the HTC conditions best suited to obtain hydrochar with maximal gasification activity.

2. Materials And Methods

2.1. Materials

Dewatered SS with a moisture content of ~80 wt%, collected from a wastewater treatment plant in Jilin City, Jilin Province, China, was stored at 4 °C and used as the raw material for HTC. For characterization, SS was dried at 105 °C for 24 h, ground into fine powder, and sealed in a dry glass bottle for subsequent analysis. Table 1 lists the primary properties of raw SS. The high content volatiles were the main source of heat released during sludge thermochemical conversion, and the ash components were mainly SiO_2, Al_2O_3, and Fe_2O_3.

Table 1. Main characteristics of the employed sludge.

Sample	Ultimate analysis (wt%, db*)				Proximate analysis (wt%, db)			HHV (kJ kg^{-1})
	C	H	N	S	Volatiles	Fixed C	Ash	
Sludge	19.68	3.33	2.99	0.62	32.88	5.78	61.34	8200

Ash (wt%)	SiO_2	Al_2O_3	Fe_2O_3	P_2O_5	CaO	MgO	K_2O	SO_3	Na_2O
	41.90	18.10	10.40	7.03	4.76	2.53	2.40	1.58	1.21

*db = dry basis.

2.2. HTC experiments

HTC experiments were carried out in a 0.5-L stirred batch reactor (stainless steel 316 L, GCF-type, Dalian Controlled Plant, China). In each experiment, the reactor was charged with a mixture of SS (20 g) and deionized water (200 mL). In experiments involving acid catalysis, SS (20 g) was mixed with acetic acid solutions (200 mL) of different concentrations. The reactor was sealed, purged with N_2 to remove residual air, heated to the predetermined temperature (160, 210, or 260 °C) using an electric heater, and held at this temperature for a certain time (30, 90, or 150 min). The reaction pressure (that of water alone at the respective temperature) ranged from 1.6 to 4.7 MPa. After the reaction, the slurry samples were collected and separated into filtrates and hydrochar by filtration. After 24-h drying at 60 °C, hydrochar was ground into fine powder and stored in an enclosed plastic pipe until analysis. Hydrochar samples were denoted as "HC-*A*-*B*-*C*," where *A* is the HTC temperature, *B* is the HTC residence time, and *C* is the acetic acid concentration. Two indexes (hydrochar mass yield (H_y) and HHV) were selected as dependent variables representing responses to HTC condition variation.

H_y was estimated using Eq. (1), while HHV was estimated by bomb calorimetry (SDAC6000, Hunan Sundy Science and Technology Co., Ltd., China). The nitrogen, hydrogen, and carbon contents of hydrochar were determined by combustion at 950 °C employing an automatic elemental analyzer (EA3000, Euro Vector S.P.A., Italy).

H_y (%) = 100% × weight of dry hydrochar/weight of dry raw material. (1)

2.3. CO_2-assisted gasification experiments

Hydrochar gasification was carried out in a micro-fluidized bed reaction analyzer coupled with a mass spectrometer (MFBRA-MS). The assembly mainly comprised a gas supply system, a gasification system, and an online gas monitoring and analysis system (Fig. 1).

Gasification was performed as follows. (1) The reactor was heated to 800 °C. (2) Hydrochar (10 mg) was placed into the feeding pipe. (3) The gasification agent (99.999 vol% CO_2) was supplied to the reactor at a flow rate of 0.5 L min^{-1} to stabilize the gas baseline. (4) The pulse was turned on through the solenoid valve, and the sample was instantly sprayed into the reaction area. The gas was analyzed using an online mass spectrometer. (5) Procedures (2)–(4) were repeated until all experiments were completed.

The carbon conversion of hydrochar gasification (X) was calculated as

$$X = \frac{\int_{t_0}^{t} \psi_i \times q_v \, dt}{\int_{t_0}^{t_d} \psi_i \times q_v \, dt}, \quad (2)$$

where t is the reaction time (s), t_0 is the initial reaction time (s), t_d is the end reaction time, ψ_i is the volume fraction of component i in the produced gas (%), and q_v is the flow rate (mol min^{-1}).

To establish a relationship between HTC conditions and hydrochar gasification reactivity, we used RSM to optimize this reactivity and thus obtain optimal HTC conditions. The reaction index $R_{0.9}$, employed to quantitatively characterize the overall gasification reactivity of hydrochar, was determined as

$R_{0.9} = 0.9/t_{X=0.9}$, (3)

where $t_{X=0.9}$ represents the gasification time (min) required for a carbon conversion of 0.9.

2.4. Experimental design for process optimization

RSM is a method of optimizing experimental conditions, which is suitable for solving the related problems of nonlinear data processing. By means of regression fitting and response surface drawing, the predicted optimal response value and corresponding experimental conditions can be found out.

Experiments were designed using the Box–Behnken method, a typical RSM technique that is usually used to optimize response-affecting process parameters.

To determine the optimum HTC conditions for hydrochar production, we investigated the effects of three factors (reaction temperature, residence time, and acetic acid concentration) and optimized them within the ranges of

160–260 °C, 30–150 min, and 0–3.0 M, respectively, to maximize the yield and HHV of SS hydrochar. The relationship between HTC conditions and gasification performance was investigated using the gasification activity index as the optimization goal under different HTC conditions.

The experimental design was carried out using Design-Expert.V8.0.6.1 data analysis software (Stat-Ease, Inc). The optimization conditions and objectives of HTC and gasification processes are presented in Tables 2 and 3.

Table 2. RSM design parameters and optimization objectives of HTC.

Run	*A*: HTC temperature (°C)	*B*: Residence time (min)	*C*: Acetic acid concentration (M)
1	260	90	3
2	210	30	0
3	210	90	1.5
4	160	90	0
5	210	90	1.5
6	260	150	1.5
7	210	150	0
8	160	90	3
9	210	90	1.5
10	210	90	1.5
11	210	150	3
12	160	30	1.5
13	160	150	1.5
14	260	90	0
15	210	90	1.5
16	260	30	1.5
17	210	30	3

Table 3. RSM design parameters and optimization objectives of SS hydrochar gasification.

Run	*A*: HTC temperature (°C)	*B*: Residence time (min)	*C*: Acetic acid concentration (M)
1	260	90	3
2	210	30	0
3	210	90	1.5
4	160	90	0
5	210	90	1.5
6	260	150	1.5
7	210	150	0
8	160	90	3
9	210	90	1.5
10	210	90	1.5
11	210	150	3
12	160	30	1.5
13	160	150	1.5
14	260	90	0
15	210	90	1.5
16	260	30	1.5
17	210	30	3

3. Results And Discussion

3.1. Analysis of hydrochar characteristics

Table 4 lists the fuel characteristics of hydrochar obtained under different HTC conditions. Compared with raw SS, hydrochar obtained at 160°C had a higher carbon content regardless of residence time and acetic acid concentration. Whereas carbon and hydrogen contents decreased with increasing HTC temperature and residence time, as observed by Zhang et al. (Zhang et al. 2019), the opposite trend was observed for nitrogen content (e.g., HC-260-90 was more nitrogen-rich than HC-210-30), which was ascribed to the occurrence of nitrogen absorption at higher temperatures and longer reaction times (He et al. 2013; Wang et al. 2020). The decrease in the contents of carbon, hydrogen, and nitrogen observed in the presence of acetic acid was ascribed to its promotional effect on hydrolysis. At high temperatures and long residence times, SS hydrolysis also produces organic (e.g., acetic, formic, levulinic, and glycolic) acids, the presence of which in the liquid phase catalyzed decarboxylation and dehydration reactions (Stemann et al. 2013). According to all the above analysis, different HTC conditions have different effects on the properties of hydrochar. To maximize the fuel performance of hydrochar, we optimized hydrochar yield and HHV by RSM.

Table 4
Basic fuel characteristics of hydrochar.

Run	C ($_{ad}$%)	H ($_{ad}$ %)	N ($_{ad}$ %)	Hydrochar yield (wt%)	HHV (kJ kg^{-1})
1	15.07	1.79	1.36	55	5885.97
2	15.72	2.05	1.1	76	6228.26
3	14.2	2.19	0.78	63	6433.76
4	20.24	3.03	2.14	82.69	7725.37
5	14.51	2.1	0.8	65	6489.69
6	12.88	1.74	0.69	51.5	5478.26
7	16.14	2.05	1.63	73.1	6193.58
8	21.25	3.08	2.37	73.63	8425.62
9	14.89	2.18	0.75	65	6323.92
10	14.76	2.15	0.77	65	6377.54
11	14.64	1.95	0.76	65	6675.47
12	19.36	3.04	1.99	74.2	8321.88
13	20.64	3.09	1.69	74.3	8311.86
14	14.06	1.9	1.35	63.9	5586.66
15	14.51	2.14	0.78	66	6370.44
16	15	2.04	0.77	57	6114.73
17	15.76	2.19	0.82	68	6787.71

3.2. Optimization of hydrochar yield and HHV

3.2.1 Analysis of variance (ANOVA) and model building

In the experimental process, only 17 groups of experimental conditions were selected, which could not intuitively obtain the optimal conditions. Through response surface analysis, the functional relationship between response target and factors can be established, and the response surface diagram can be used to display the functional relationship, and the optimal reaction condition can be obtained.

Firstly, regression analysis was carried out on the experimental results. The results of model variance analysis, presented in Tables 5 and 6, the *F*-values of the model equaled 168.2856 and 132.086, while the *p*-values were less than 0.05, and the lack of fit item is greater than 0.05, indicating that the model item is significant. Figs. 2a and 2b compare actual values with predicted values, revealing that the deviation between them was small and thus showing that the regression model could well predict the hydrochar HHV and yield.

Table 5
ANOVA of the regression model used to predict hydrochar mass yield.

Source	SS	df	MS	*F*-value	*p*-value	
Model	1035.21	9	115.0233	132.086	< 0.0001	significant
A: Temperature	749.2321	1	749.2321	860.3739	< 0.0001	
B: Residence time	15.96125	1	15.96125	18.32896	0.0036	
C: Acetic acid concentration	145.0105	1	145.0105	166.5215	< 0.0001	
AB	7.84	1	7.84	9.002994	0.0199	
AC	0.0064	1	0.0064	0.007349	0.9341	
BC	0.0025	1	0.0025	0.002871	0.9588	
A^2	5.424105	1	5.424105	6.228723	0.0412	
B^2	1.440947	1	1.440947	1.654699	0.2392	
C^2	111.2404	1	111.2404	127.7419	< 0.0001	
Residual	6.09575	7	0.870821			
Lack of fit	1.29575	3	0.431917	0.359931	0.7862	not significant
Pure error	4.8	4	1.2			
total	1041.306	16				

df: degrees of freedom; SS: sum of squares (Total)=sum of squares(Model)+sum of squares(Residual); MS: mean squares=SS/df; *F*-value: Fisher test value= MS(Model)/MS(Residual); *p*-value: the probability when the value is bigger than *F*-value.

Table 6
ANOVA of the regression model used to predict hydrochar HHV.

Source	SS	df	MS	*F*-value	*p*-value	
Model	13885669	9	1542852	168.2856	< 0.0001	significant
A: Temperature	1180763	1	11807637	1287.91	< 0.0001	
B: Residence time	78687.43	1	78687.43	8.582781	0.0220	
C: Acetic acid concentration	520659.1	1	520659.1	56.79056	0.0001	
AB	98109.9	1	98109.9	10.70127	0.0137	
AC	40188.22	1	40188.22	4.383504	0.0746	
BC	1503.888	1	1503.888	0.164036	0.6976	
A^2	1255829	1	1255829	136.9787	< 0.0001	
B^2	52328.71	1	52328.71	5.707721	0.0482	
C^2	6501.875	1	6501.875	0.709188	0.4275	
Residual	64176.4	7	9168.058			
Lack of fit	47830.28	3	15943.43	3.901458	0.1108	not significant
Pure error	16346.12	4	4086.53			
total	1394984	16				

In general, the regression model of HHV and yield could be used for subsequent response surface analysis. The model formulated in terms of actual factors for H_y (%) and HHV (kJ kg^{-1}) is given by Eqs. (4) and (5):

$$H_y\ (\%) = 60.8 - 9.68A - 1.41B - 4.26C - 1.40AB + 0.04AC - 0.025BC - 1.14A^2 + 0.58B^2 + 5.14C^2, \quad (4)$$

$$\text{HHV}\ (\%) = 6399.07 - 1214.89A - 99.18B + 255.11C - 156.61AB - 100.24AC - 19.39BC + 546.13A^2 + 111.48B^2 - 39.30C^2. \quad (5)$$

In the above and subsequent equations, *A*, *B*, and *C* stand for HTC temperature (°C), residence time (min), and acetic acid concentration (M), respectively.

3.2.2 Response surface analysis of hydrochar yield

Hydrochar yield was negatively correlated with all three of these parameters, with the largest and smallest effects observed for temperature and residence time, respectively (Fig. 3). In particular, hydrochar yield decreased by 15, 10, and 5% as the reaction temperature, acetic acid concentration, and residence time increased from 160 to 260°C, 0 to 3 M, and 30 to 150 min, respectively.

The increase in the above three parameters promoted the thermal decomposition and dissolution of sludge macromolecules and thus decreased solid yield. The rise in temperature decreased the viscosity of water and thus facilitated its penetration into pores of hydrochar to promote biomass degradation (Funke et al. 2010; Wang et al.

2018). The largest decrease in hydrochar yield was observed when the reaction temperature increased from 210 to 260°C. According to Reza et al., this decrease was primarily due to the significant breakdown of hemicellulose and lignin in this temperature range and the large number of cellulose decomposition reactions above 210°C (Toufiq et al. 2016). Alternatively, the negative correlation between temperature and hydrochar yield was ascribed to the facts that (i) SS contains numerous nitrogen-containing compounds such as proteins, which, together with sugar hydrolysates, are dissolved in the aqueous phase (Wang et al. 2019) and (ii) hydrochar is difficult to produce by the thermal decomposition of proteins at ~250°C. Temperature also had a larger effect on mass yield than organic acids. Acetic acid is the main organic acid produced during HTC through the hydrolysis and dehydration of straight-chain polymers such as cellulose and hemicellulose or simple monomers in the presence of subcritical water (Liu et al. 2020). The presence of organic acids increases the concentration of protons or hydroxide ions, thus increasing the total ion concentration and promoting decarboxylation and dehydration (Reza et al. 2015). Acids also enhance dehydration, which is the main carbonization mechanism, and thus significantly decrease the oxygen content of hydrochar. It has been reported that hydrochar yield can be increased by decreasing the reaction time (Saetea et al. 2013), which is in line with our results. This behavior was ascribed to the depolymerization of biomacromolecules in SS and the further degradation of the resultant intermediates via cleavage, dehydration, decarboxylation, and deamination at long residence times.

3.2.3 Response surface analysis of hydrochar HHV

3.2.4 Results of process optimization

The optimization of HTC conditions is important for hydrochar recovery, especially from the perspective of process development. Ideally, maximal hydrochar yield and HHV should be obtained under mild conditions. The limiting conditions and results of hydrochar HHV and yield optimization are listed in Tables 7 and 8.

Table 7
Limiting conditions for hydrochar HHV and yield optimization.

Name	Goal	Lower limit	Upper limit	Lower weight	Upper weight
A: Temperature	is in range	160	260	1	1
B: Time	is in range	30	150	1	1
C: Acetic acid concentration	is in range	0	3	1	1
HHV	minimize	5478.26	8425.62	1	1
Hydrochar yield	minimize	51.5	82.69	1	1

Table 8
Results of hydrochar HHV and yield optimization.

Temperature	Time	Acetic acid concentration	HHV	Hydrochar yield	Desirability
160	30	0.07	7820.99	82.69	1
160	32.28	0.06	7814.2	82.69	1
160	37.29	0.06	7800.59	82.69	1
160	38.64	0.05	7797.23	82.69	1
160	48.65	0.04	7776.55	82.69	1
...	...	...	...	...	...

According to the prediction results, optimal conditions corresponded to an HTC temperature of 160°C, a residence time of 30 min, and an acetic acid concentration of 0.07 M, with the yield and HHV of hydrochar obtained under these conditions equaling 82.69% and 7820.99 kJ kg^{-1}, respectively. In the replication experiment conducted under these conditions, the hydrochar yield and HHV were determined as 83.07% and 7794.25 kJ kg^{-1}, respectively, deviating from the predicted values by 0.46 and 0.34%, respectively. The good agreement between simulated and experimental results confirmed the high reliability of our prediction.

The above results indicate that SS hydrochar can be used as a fuel for combustion, pyrolysis, and gasification. Among these applications, combustion is relatively simple but may produce gaseous pollutants. Therefore, the next section compares the release of gaseous pollutants in different combustion atmospheres.

3.3. Release of gaseous pollutants in different combustion atmospheres

The above analysis results show that SS hydrochar holds great promise as a combustion fuel. However, as gaseous pollutants are inevitably produced during conversion, alternatives featuring lower pollutant emissions are highly sought after. This section explores the release of nitrogen- and sulfur-containing gases during hydrochar combustion in O_2 (99.999 vol%) and CO_2 (99.999 vol%) atmospheres. As shown in Fig. 5, when hydrochar was burned in an O_2 atmosphere, the peaks of sulfur- and nitrogen-containing gases were more intense than those observed in a CO_2 atmosphere. In particular, almost no peak of sulfur-containing gas was observed in the latter case. Therefore, the gasification of hydrochar in a CO_2 atmosphere seems to be a promising thermal conversion method. The next section focuses on the gasification characteristics of hydrochar.

3.4 Analysis of CO_2 gasification characteristics

3.4.1 CO_2 emission due to combustion of residual char obtained in different gasification atmospheres

Figure 6 shows the release of CO_2 upon the combustion of residual char obtained after the completion of hydrochar gasification in Ar and CO_2 atmospheres, revealing that more CO_2 (and hence, a lower carbon

conversion) was obtained in the former case. Therefore, the CO_2 atmosphere was concluded to be more suitable for gasification reactions than inert (e.g., Ar) atmospheres.

3.4.2 Analysis of gaseous product evolution

Figure 8. Effects of (a) temperature, (b) residence time, and (c) acetic acid concentration on the release of gaseous products during CO_2-assisted gasification.

With increasing HTC temperature and residence time, the amount of released gas decreased.

HTC temperature had the largest influence on gas release and was negatively correlated with the contents of CO, CH_4, and H_2 (Fig. 8a), as high temperatures aggravated sludge hydrolysis and increased the content of soluble carbon in the aqueous phase (Yu et al. 2018). Notably, the density and dielectric constant of water decreased with increasing temperature, whereas the ionic product significantly increased (Watanabe et al. 2004), which primarily contributed to the cleavage of hydrogen bonds and hydrolysis (Wang et al. 2019). In addition, high HTC temperatures favor the aromatization of hydrochar and thus make it more thermally stable and difficult to decompose during gasification. Residence time is an important parameter influencing hydrochar formation, and long times led to the polymerization of fragments dissolved in the liquid phase, which resulted in the formation of secondary hydrochar with a polyaromatic structure (Wüst et al. 2019; Kang et al. 2012). Therefore, it can be seen from Fig. 8b shows that with the increase of the hydrothermal residence time, the content of CO and CH_4 produced by gasification decreases, and the residence time has little effect on H_2. The addition of acetic acid reduced the amount of released gaseous products (Fig. 8c). Acidic environments favor the isomerization, dehydration, and cracking (open-loop and C–C bond breakage) of SS (Liua et al. 2020). During hydrothermal processing, the decomposition of intermediates produces a large number of organic acids and thus reduces the pH of the reaction medium, while the resulting acidic environment favors the further decomposition of intermediates and the formation of a more stable double bond structure, thus promoting hydrochar aromatization (Sevill et al. 2009).

3.4.3 Analysis of conversion during hydrochar gasification

Figure 9 shows the effect of time on conversion during CO_2-assisted hydrochar gasification, revealing that compared with raw SS, hydrochar required less time to reach a conversion of unity, i.e., the gasification activity of sludge increased after HTC. Moon et al. (Moon et al. 2015) showing that the rise in the lignin content of SS after HTC helped to increase the production of methane during gasification and allowed this gasification to be completed in a shorter time. At 160°C and 260°C, the conversion of hydrochar was lower than that of raw SS, but at the intermediate temperature (210°C), the conversion is higher. Moreover, hydrochar gasification reactivity increased with increasing residence time and acetic acid concentration.

3.4.4 Analysis of the gasification activity optimization of hydrochar

The ANOVA results for the regression model used to predict the gasification activity index are shown in Table 9. The *p*-value of the employed model was less than 0.05, and the model lack-of-fit ($p > 0.05$) was insignificant. Figure 10 compares the predicted results with the experimental results, and the $adj.R^2$ is 0.993, indicating that the difference between the two is small and the fitting degree is high.In the working condition 160-90-1.5, the value of

$R_{0.9}$ is the largest, so it is distributed in the upper right corner. The quadratic regression equation used to calculate this index is given below.

$$R_{0.9}\ (s^{-1}) = 0.2876 + 0.006A - 0.002B + 0.0061C + 0.0032AB - 0.0204AC - 0.0039BC - 0.086A^2 - 0.0367B^2 - 0.0503C^2. \quad (6)$$

Table 9
ANOVA of the regression model used to predict the gasification activity index.

Source	*SS*	*df*	MS	*F- value*	*p-value*	
Model	0.05454	9	0.00606	991.2505	< 0.0001	significant
A: Temperature	0.000283	1	0.000283	46.36046	0.0003	
B: Time	3.66E-05	1	3.66E-05	5.984332	0.0443	
C: Acetic acid concentration	0.000296	1	0.000296	48.41328	0.0002	
AB	4.16E-05	1	4.16E-05	6.809475	0.0349	
AC	0.00167	1	0.00167	273.1828	< 0.0001	
BC	6.22E-05	1	6.22E-05	10.17782	0.0153	
A^2	0.031132	1	0.031132	5092.356	< 0.0001	
B^2	0.005681	1	0.005681	929.1869	< 0.0001	
C^2	0.010665	1	0.010665	1744.561	< 0.0001	
Residual	4.28E-05	7	6.11E-06			
Lack of fit	3.2E-05	3	1.07E-05	3.949926	0.1088	not significant
Pure error	1.08E-05	4	2.7E-06			
total	0.054583	16				

Figure 11. Response surface maps (a, c, e) and contour maps (b, d, f) showing the effects of temperature, residence time, and acetic acid concentration on the gasification activity index of hydrochar.

Table 10
Limiting conditions for the optimization of the hydrochar gasification activity index.

Name	Goal	Lower limit	Upper limit	Lower weight	Upper weight
A: Temperature	is in range	160	260	1	1
B: Time	is in range	30	150	1	1
C: Acetic acid concentration	is in range	0	3	1	1
Reactivity index	maximize	0.12	0.29	1	1

Table 11
Results of optimization of the hydrochar gasification activity index.

Number	HTC temperature (°C)	Residence time (min)	Acetic acid concentration (M)	$R_{0.9}$ (s^{-1})	Desirability	
1	211.34	88.16	1.58	0.29	0.99	Selected

The results optimization of activity index listed in Tables 10 and 11. According to the predicted results, the highest gasification activity index (0.29 s^{-1}) was obtained at an HTC temperature of 211.34°C, a residence time of 88.16 min, and an acetic acid concentration of 1.58 M. When a replication experiment was conducted under the above conditions, $R_{0.9}$ was obtained as 0.28 s^{-1}, deviating from the predicted value by 2.19%, which was within the error range. Compared with those required to obtain high-quality hydrochar (160°C, 30 min, 0.07 M) as solid fuel in Section 3.2.3, the optimized conditions for hydrochar gasification (211.34°C, 88.16 min, 1.58 M) were more severe. Milder HTC conditions allowed hydrochar to retain more carbon and some soluble organic matter and thus maximize the HHV and yield, whereas harsher conditions favored hydrochar pore development and alkali metal retention, thus promoting catalytic gasification.

4. Conclusions

The main objective of this work is to convert the sludge into a usable bioenergy feedstock by hydrothermal carbonization. The main results are as follows.

(1) With increasing HTC temperature, residence time, and acetic acid concentration, the carbon, hydrogen, and nitrogen contents of hydrochar decreased. The highest hydrochar yield and HHV were obtained under mild conditions.

(2) The conditions affording maximal HHV and yield corresponded to 160°C, 30 min, and 0.07 M acetic acid. Under these conditions, the hydrochar yield and HHV were predicted to equal 82.69% and 7820.99 kJ kg^{-1}, respectively. These values deviated from the experimentally determined ones by 0.34 and 0.46%, respectively, i.e., were within the acceptable error range.

(3) HTC conditions strongly affected hydrochar gasification performance. As HTC conditions became more severe, the gasification activity index first increased and then decreased, i.e., was maximized under moderate conditions. The RSM-predicted optimal HTC conditions corresponded to 211.34°C, 88.16 min, and 1.58 M acetic acid. Under these conditions, the hydrochar gasification activity index equaled 0.29 s^{-1}.

The results of this study provide a detailed observation of SS utilization by HTC coupled with gasification and providing referential information for the design, optimization, and even upscaling of thermochemical conversion processes. However, under the expected optimization conditions, extensive experiments on SS should be the future work. In addition, a comprehensive technical and economic analysis of SS HTC process is needed to prove its scalability.

Declarations

Authors' contributions Chenchen Zhao and Shuai Guo had the idea for the article; Dandan Xu, Shuai Guo, and Xin Guo performed the literature search and data analysis; and Shuai Guo, Dandan Xu, Xin Guo, and Xingcan Li

drafted and/or critically revised the work. All authors read and approved the final manuscript.

Funding This work was supported by the National Natural Science Funds for Young Scholars of China (No. 51806033), and Jilin Provincial Science and Technology Development Program (No. 20190201096JC).

Data availability All data generated or analyzed during this study are included in this published article.

Compliance with ethical standards

Conflict of interest The authors declare that they have no conflict of interest.

Ethical approval The authors state that the research was conducted according to ethical standards.

Consent to participate Not applicable.

Consent to publish Not applicable.

References

1. Atallah E, Kwapinski W, Ahmad MN, Leahy JJ, Zeaiter J (2019) Effect of water-sludge ratio and reaction time on the hydrothermal carbonization of olive oil mill wastewater treatment: Hydrochar characterization. Journal of Water Process Engineering 31:100813. https://doi.org/10.1016/j.jwpe.2019.100813
2. Afolabi OD, Sohail M, Cheng YL (2020) Optimisation and characterisation of hydrochar production from spent coffee grounds by hydrothermal carbonization. Renewable Energy 147:1380–1391. https://doi.org/10.1016/j.renene.2019.09.098
3. Bora AP, Gupta DP, Durbha KS (2020) Sewage sludge to bio-fuel: A review on the sustainable approach of transforming sewage waste to alternative fuel. Fuel 259:116262
4. Chen SY, Zhao ZH, Soomro A, Ma SW, Wu MD, Sun Z, Xiang WG (2020) Hydrogen-rich syngas production via sorption-enhanced steam gasification of sewage sludge. Biomass Bioenerg 138:105607. https://doi.org/10.1016/j.biombioe.2020.105607
5. Escala M, Zumbühl T, Koller C, Junge R, Krebs R (2012) Hydrothermal Carbonization as an Energy-Efficient Alternative to Established Drying Technologies for Sewage Sludge: A Feasibility Study on a Laboratory Scale. Energy Fuels 27(1):454–460. https://doi.org/10.1021/ef3015266
6. Evcil T, Simsir H, Ucar S, Tekin K, Karagoz S (2020) Hydrothermal carbonization of lignocellulosic biomass and effects of combined Lewis and Brønsted acid catalysts. Fuel 279:118458. https://doi.org/10.1016/j.fuel.2020.118458
7. Franceschini G, Macchietto S (2008) Model-based design of experiments for parameter precision: State of the art. Chem Eng Sci 63:4846–4872. https://doi.org/10.1016/j.ces.2007.11.034
8. Funke A, Ziegler F (2010) Hydrothermal carbonization of biomass: a summary and discussion of chemical mechanisms for process engineering. Biofuels Bioprod Bioref 4:160–177. https://doi.org/10.1002/bbb.198
9. Gai C, Chen M, Liu T, Peng N, Liu Z (2016) Gasification characteristics of hydrochar and pyrochar derived from sewage sludge. Energy 113:957–965. https://doi.org/10.1016/j.energy.2016.07.129
10. He C, Tang C, Li C, Yuan J, Tran KQ, Bach QV, Qiu R, Yang Y (2018) Wet torrefaction of biomass for high quality solid fuel production: A review. Renew Sustain Energy Rev 91:259–271.

https://doi.org/10.1016/j.rser.2018.03.097

11. He C, Giannis A, Wang JY (2013) Conversion of sewage sludge to clean solid fuel using hydrothermal carbonization: Hydrochar fuel characteristics and combustion behavior. Appl Energy 111:257–266. https://doi.org/10.1016/j.apenergy.2013.04.084
12. Huang H, Chang Y, Lai F, Zhou C, Pan Z, Xiao X, Wang J, Zhou C (2019) Co-liquefaction of sewage sludge and rice straw/wood sawdust: The effect of process parameters on the yields/properties of bio-oil and biochar products. Energy 173:140–150. https://doi.org/10.1016/j.energy.2019.02.071
13. Kelessidis A, Stasinakis AS (2012) Comparative study of the methods used for treatment and final disposal of sewage sludge in European countries. Waste Manag 2012; 32: 1186–95. https://doi.org/10.1016/j.wasman.2012.01.012
14. Kim D, Lee K, Park KY (2014) Hydrothermal carbonization of anaerobically digested sludge for solid fuel production and energy recovery. Fuel 130:120–125. https://doi.org/10.1016/j.fuel.2014.04.030
15. Kang K, Nanda S, Sun G, Qiu L, Gu Y, Zhang T, Zhu M, Sun R (2019) Microwave-assisted hydrothermal carbonization of corn stalk for solid biofuel production: Optimization of process parameters and characterization of hydrochar. Energy 186:115795. https://doi.org/10.1016/j.energy.2019.07.125
16. Kang S, Li X, Fan J, Chang J (2012) Characterization of hydrochars produced by hydrothermal carbonization of lignin, cellulose,D-xylose, and wood meal. Ind Eng Chem Res 51:9023–9031. https://doi.org/10.1021/ie300565d
17. Lee J, Hong J, Jang D, Park KY (2019) Hydrothermal carbonization of waste from leather processing and feasibility of produced hydrochar as an alternative solid fuel. J Environ Manage 247:115–120. https://doi.org/10.1016/j.jenvman.2019.06.067
18. Liua X, Zhaia Y, Li S, Wang B, Wang T, Liu Y, Qiu Z, Li C (2020) Hydrothermal carbonization of sewage sludge: Effect of feed-water pH on hydrochar's physicochemical properties, organic component and thermal behavior. J Hazard Mater 388:122084. https://doi.org/10.1016/j.jhazmat.2020.122084
19. Lin Y, Ma X, Peng X, Yu Z, Fang S, Lin Y, Fan Y (2016) Combustion pyrolysis and char CO_2-gasification characteristics of hydrothermal carbonization solid fuel from municipal solid wastes. Fuel 181:905–915. https://doi.org/10.1016/j.fuel.2016.05.031
20. Liu X, Zhai Y, Li S, Wang B, Wang T, Liu Y, Qiu Z, Li C (2020) Hydrothermal carbonization of sewage sludge: Effect of feed-water pH on hydrochar's physicochemical properties, organic component and thermal behavior. J Hazard Mater 388:122084. https://doi.org/10.1016/j.jhazmat.2020.122084
21. Li GY, Li AQ, Zhang H, Wang JP, Chen SY, Liang YH (2018) Theoretical study of the CO formation mechanism in the CO_2 gasification of lignite. Fuel 211:353–362. https://doi.org/10.1016/j.fuel.2017.09.030
22. Liu H, Chen Y, Yang H, Gentili FG, Söderlind U, Wang X, Zhang W, Chen H (2019) Hydrothermal carbonization of natural microalgae containing a high ash content. Fuel 249:441–448. https://doi.org/10.1016/j.fuel.2019.03.004
23. Mateo-Sagasta J, Raschid-Sally L, Thebo A (2015) Global Wastewater and Sludge Production, Treatment and Use. Wastewater 15–38. http://doi.org/10.1007/978-94-017-9545-6_2
24. Meng XZ, Venkatesan AK, Ni YL, Steele JC, Wu LL, Bignert A, Bergman A, Halden RU (2016) Organic contaminants in Chinese sewage sludge: a meta-analysis of the literature of the past 30 years. Environ Sci Technol 50(11):5454–5466. https://doi.org/10.1021/acs.est.5b05583

25. Moon J, Mun TY, Yang W, Lee U, Hwang J, Jang E, Choi C (2015) Effects of hydrothermal treatment of sewage sludge on pyrolysis and steam gasification. Energy Convers Manag 103:401–407. https://doi.org/10.1016/j.enconman.2015.06.058
26. Mosqueda A, Medrano K, Gonzales H, Yoshikawa K (2019) Effect of hydrothermal and washing treatment of banana leaves on co-gasification reactivity with coal. Energy Procedia 158:785–791. https://doi.org/10.1016/j.apenergy.2019.05.008
27. Mackintosh AF, Shin T, Yang H, Choe K (2020) Hydrothermal Polymerization Catalytic Process Effect of Various Organic Wastes on Reaction Time, Yield, and Temperature. Processes 8(3):303. https://doi.org/10.3390/pr8030303
28. Ma J, Chen M, Yang T, Liu Z, Jiao W, Li D, Gai C (2019) Gasification performance of the hydrochar derived from co-hydrothermal carbonization of sewage sludge and sawdust. Energy 173:732–739. https://doi.org/10.1016/j.energy.2019.02.103
29. Mosqueda A, Wei J, Medrano K, Gonzales H, Ding L, Yu G, Yoshikawa K (2019) Co-gasifcation reactivity and synergy of banana residue hydrochar and anthracite coal blends. Appl Energy 250:92–97. https://doi.org/10.1016/j.apenergy.2019.05.008
30. Park KY, Lee K, Kim D (2018) Characterized hydrochar of algal biomass for producing solid fuel through hydrothermal carbonization. Biores Technol 258:119–124. https://doi.org/10.1016/j.biortech.2018.03.003
31. Peng C, Zhai Y, Zhu Y, Xu B, Wang T, Li C, Zeng G (2016) Production of char from sewage sludge employing hydrothermal carbonization: Char properties, combustion behavior and thermal characteristics. Fuel 176:110–118. https://doi.org/10.1016/j.fuel.2016.02.068
32. Parvez AM, Mujtaba IM, Wu T (2016) Energy, exergy and environmental analyses of conventional, steam and CO_2-enhanced rice straw gasification. Energy 94:579–588. https://doi.org/10.1016/j.energy.2015.11.022
33. Reza MT, Wirth B, Lüder U, Werner M (2014) Behavior of selected hydrolyzed and dehydrated products during hydrothermal carbonization of biomass. Bioresour Technol 169:352–361. https://doi.org/10.1016/j.biortech.2014.07.010
34. Reza MT, Rottler E, Herklotz L, Wirth B (2015) Hydrothermal carbonization (HTC) of wheat straw: Influence of feedwater pH prepared by acetic acid and potassium hydroxide. Biores Technol 182:336–344. https://doi.org/10.1016/j.biortech.2015.02.024
35. Sharma HB, Sarmah AK, Dubey B (2020) Hydrothermal carbonization of renewable waste biomass for solid biofuel production: A discussion on process mechanism, the influence of process parameters, environmental performance and fuel properties of hydrochar. Renew Sustain Energy Rev 123:109761. https://doi.org/10.1016/j.rser.2020.109761
36. Stemann J, Putschew A, Ziegler F (2013) Hydrothermal carbonization: Process water characterization and effects of water recirculation. Biores Technol 143:139–146. https://doi.org/10.1016/j.biortech.2013.05.098
37. Saetea P, Tippayawong N (2013) Recovery of value-added products from hydrothermal carbonization of sewage sludge. ISRN Chem Eng 2013:1–6. https://doi.org/10.1155/2013/268947
38. Shen Y, He C, Chen X, Lapkin AA, Xiao W, Wang CH (2018) Nitrogen removal and energy recovery from sewage sludge by combined hydrothermal pretreatment and CO_2 gasification. ACS Sustainable Chemistry Engineering 6(12):16629–16636. https://doi.org/10.1021/acssuschemeng.8b03857
39. Sun Y, Zhang Z, Liu L, Wang X (2015) Integrated carbon dioxide/sludge gasification using waste heat from hot slags: syngas production and sulfur dioxide fixation. Bioresour Technol 181:174–182.

https://doi.org/10.1016/j.biortech.2015.01.061

40. Sevill M, Fuertes AB (2009) The production of carbon materials by hydrothermal carbonization of cellulose. Carbon 47:2281–2289. https://doi.org/10.1016/j.carbon.2009.04.026
41. Toufiq Reza M, Freitas A, Yang X, Hiibel S, Lin H, Coronella CJ (2016) Hydrothermal carbonization (HTC) of cow manure: Carbon and nitrogen distributions in HTC products. Environmental Progress Sustainable Energy 35(4):1002–1011. https://doi.org/10.1002/ep.12312
42. Tasca AL, Puccini M, Gori R, Corsi I, Galletti AMR, Vitolo S (2019) Hydrothermal carbonization of sewage sludge: A critical analysis of process severity, hydrochar properties and environmental implications. Waste Manag 93:1–13. https://doi.org/10.1016/j.wasman.2019.05.027
43. Venkatesan AK, Done HY, Halden RU (2015) United States national sewage sludge repository at Arizona State University-a new resource and research tool for environmental scientists, engineers, and epidemiologists. Environ Sci Pollut Res 22:1577–1586. https://doi.org/10.1007/s11356-014-2961-1
44. Wang L, Li A, Chang Y (2015) Hydrothermal treatment coupled with mechanical expression at increased temperature for excess sludge dewatering: The dewatering performance and the characteristics of products. Water Res 68:291–303. https://doi.org/10.1016/j.watres.2014.10.016
45. Wei J, Guo Q, Ding L, Yoshikawa K, Yu G (2017) Synergy mechanism analysis of petroleum coke and municipal solid waste (MSW)-derived hydrochar co-gasification. Appl Energy 206:1354–1363. https://doi.org/10.1016/j.apenergy.2017.10.005
46. Wang C, Fan Y, Hornung U, Zhu W, Dahmen N (2020) Char and tar formation during hydrothermal treatment of sewage sludge in subcritical and supercritical water: Effect of organic matter composition and experiments with model compounds. J Clean Prod 242:118586. https://doi.org/10.1016/j.jclepro.2019.118586
47. Wang T, Zhai Y, Zhu Y, Li C, Zeng G (2018) A review of the hydrothermal carbonization of biomass waste for hydrochar formation: Process conditions, fundamentals, and physicochemical properties. Renew Sustain Energy Rev 90:223–247. https://doi.org/10.1016/j.rser.2018.03.071
48. Wang L, Chang Y, Liu Q (2019) Fate and distribution of nutrients and heavy metals during hydrothermal carbonization of sewage sludge with implication to land application. J Clean Prod 225:972–983. https://doi.org/10.1016/j.jclepro.2019.03.347
49. Watanabe M, Sato T, Inomata H, Smith RL Jr, Kruse KA Jr, Dinjus E (2004) Chemical reactions of C_1 compounds in near-critical and supercritical water. Chem Rev 104:5803–5822. https://doi.org/10.1002/chin.200511294
50. Wang L, Chang Y, Li A (2019) Hydrothermal carbonization for energy-efficient processing of sewage sludge: A review. Renew Sustain Energy Rev 108:423–440. https://doi.org/10.1016/j.rser.2019.04.011
51. Wüst D, Rodriguez Correa C, Suwelack KU, Köhler H, Kruse A (2019) Hydrothermal carbonization of dry toilet residues as an added-value strategy – Investigation of process parameters. J Environ Manage 234:537–545. https://doi.org/10.1016/j.jenvman.2019.01.005
52. Wei J, Guo Q, Song X, Ding L, Mosqueda A, Liu Y, Yoshikawa K, Yu G (2020) Effect of hydrothermal carbonization temperature on reactivity and synergy of co-gasification of biomass hydrochar and coal. Appl Therm Eng 183:116232. https://doi.org/10.1016/j.applthermaleng.2020.116232
53. Yu Y, Lei Z, Yang X, Yang X, Huang W, Shimizu K, Zhang Z (2018) Hydrothermal carbonization of anaerobic granular sludge: Effect of process temperature on nutrients availability and energy gain from produced hydrochar. Appl Energy 229:88–95. https://doi.org/10.1016/j.apenergy.2018.07.088

54. Zheng XY, Jiang ZW, Ying Z, Song JX, Wang B (2020) Role of feedstock properties and hydrothermal carbonization conditions on fuel properties of sewage sludge-drived hydrochar using multiple linear regression technique. Fuel 271:117609. https://doi.org/10.1016/j.fuel.2020.117609
55. Zhao P, Shen Y, Ge S, Chen Z, Yoshikawa K (2014) Clean solid biofuel production from high moisture content waste biomass employing hydrothermal treatment. Appl Energy 131:345–367. https://doi.org/10.1016/j.apenergy.2014.06.038
56. Zheng X, Chen W, Ying Z, Huang J, Ji S, Wang B (2019) Thermodynamic investigation on gasification performance of sewage sludge-derived hydrochar: Effect of hydrothermal carbonization. Int J Hydrogen Energy 44(21):10374–10383. https://doi.org/10.1016/j.ijhydene.2019.02.200
57. Zhang Y, Jiang Q, Xie W, Wang Y, Kang J (2019) Effects of temperature, time and acidity of hydrothermal carbonization on the hydrochar properties and nitrogen recovery from corn stover. Biomass Bioenerg 122:175–182. https://doi.org/10.1016/j.biombioe.2019.01.035
58. Zhu Z, Rosendahl L, Toor SS, Yu D, Chen G (2015) Hydrothermal liquefaction of barley straw to bio-crude oil: Effects of reaction temperature and aqueous phase recirculation. Appl Energy 137:183–192. https://doi.org/10.1016/j.apenergy.2014.10.005
59. Zhang X, Gao B, Zhao S, Wu P, Han L, Liu X (2020) Optimization of a “coal-like” pelletization technique based on the sustainable biomass fuel of hydrothermal carbonization of wheat straw. J Clean Prod 242:118426. https://doi.org/10.1016/j.jclepro.2019.118426

Figures

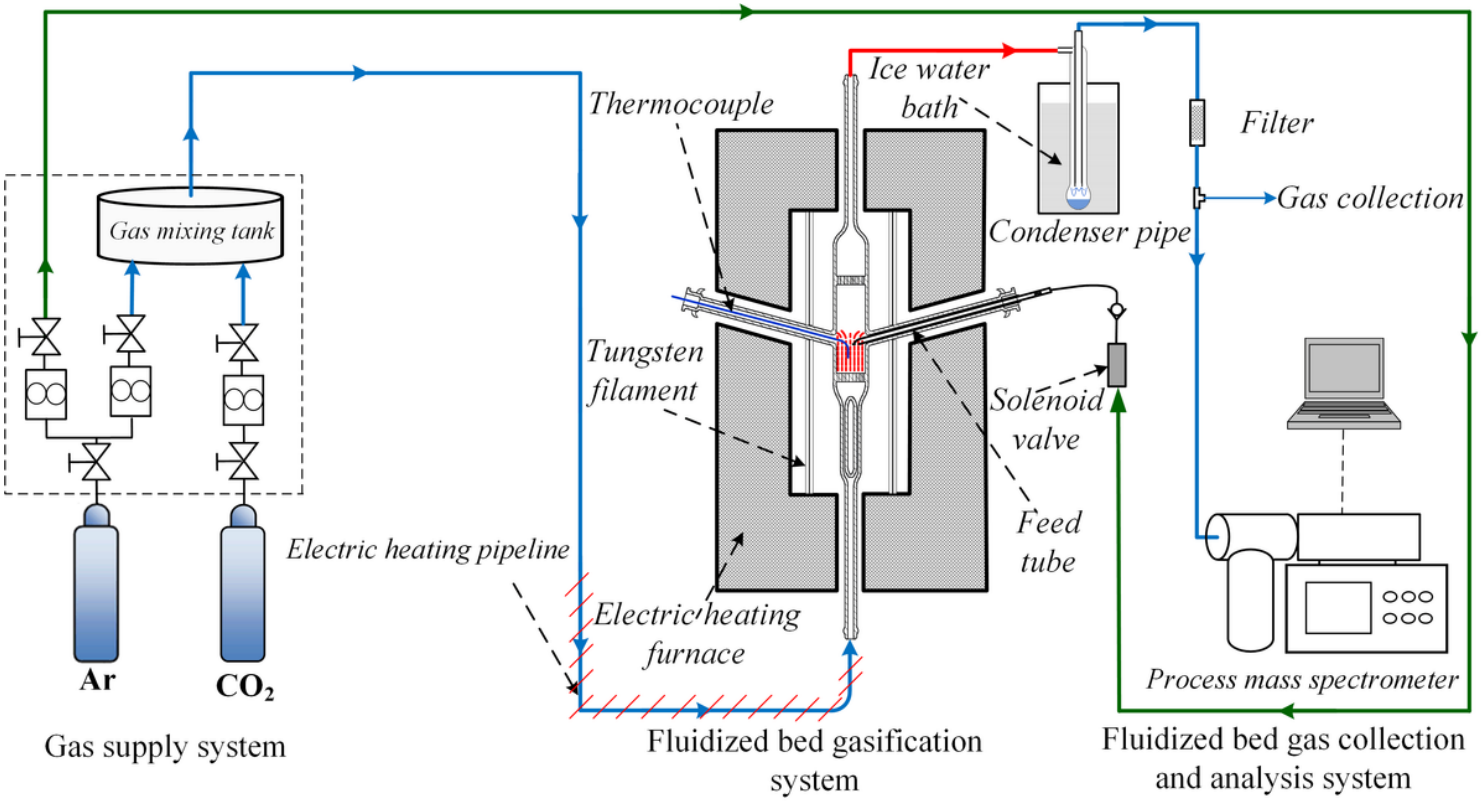

Figure 1

Schematic diagram of MFBRA-MS.

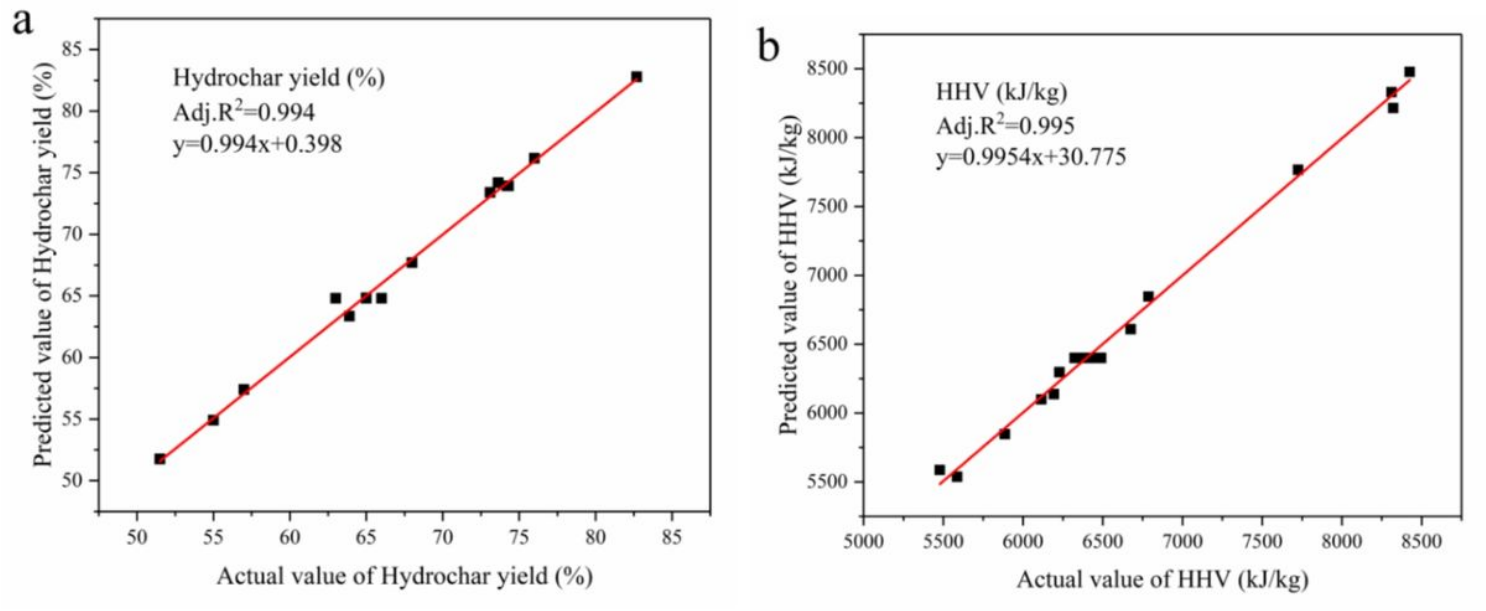

Figure 2

Comparison of actual and predicted (a) yields and (b) HHVs of hydrochar.

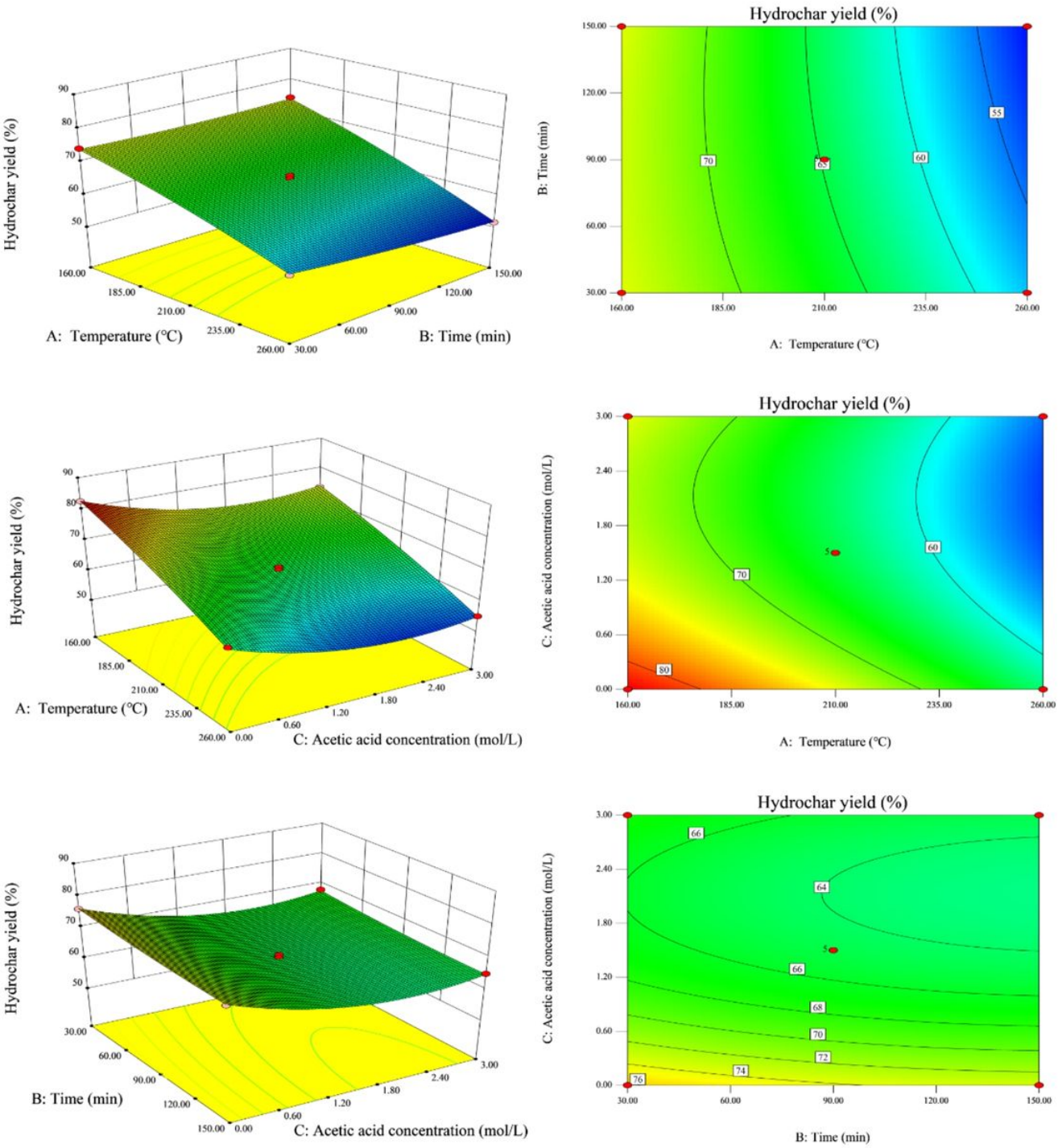

Figure 3

Response surface maps (a, c, e) and contour maps (b, d, f) showing the effects of temperature, residence time, and acetic acid concentration on hydrochar yield.

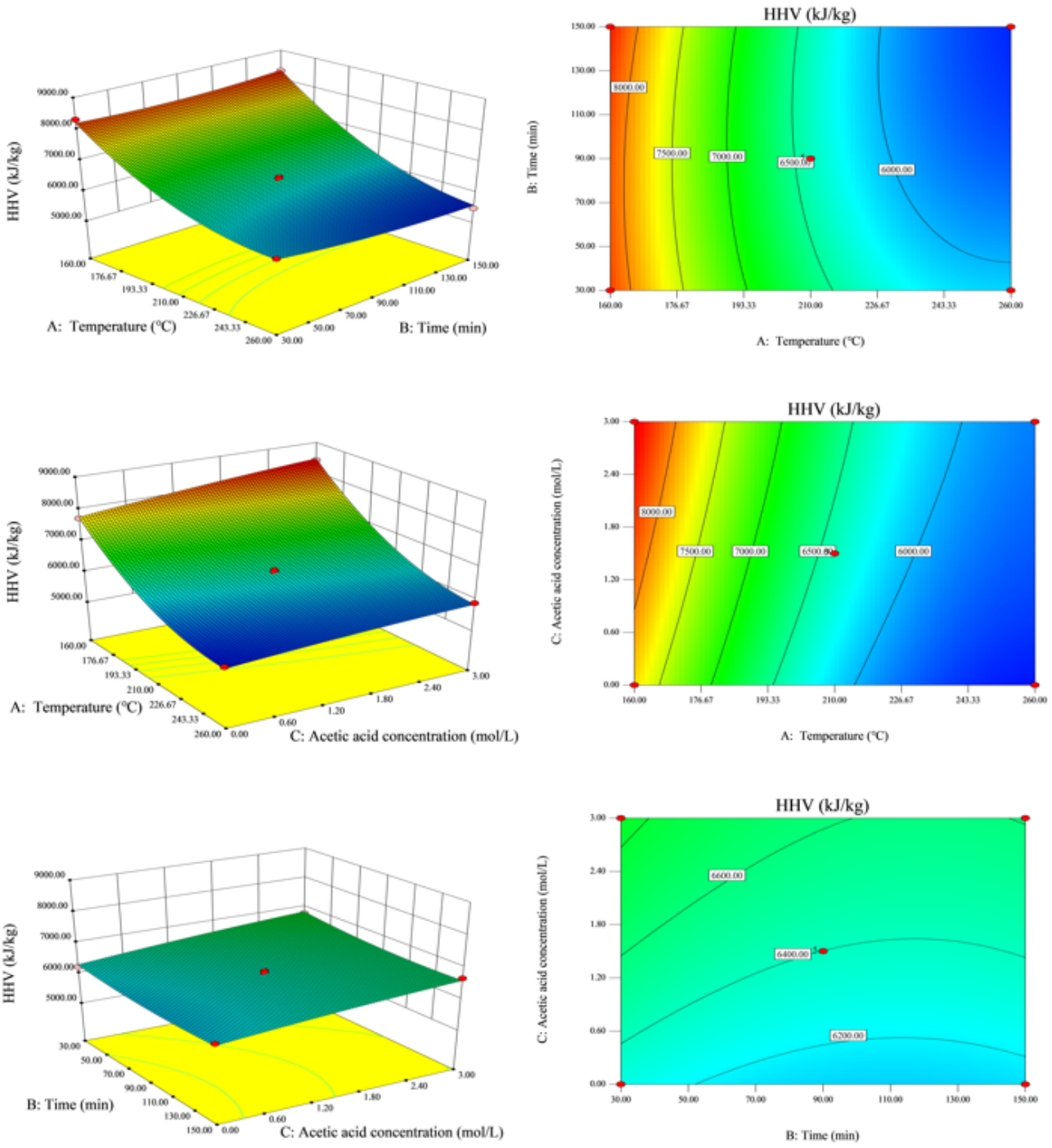

Figure 4

Response surface maps (a, c, e) and contour maps (b, d, f) showing the effects of temperature, residence time, and acetic acid concentration on hydrochar HHV.

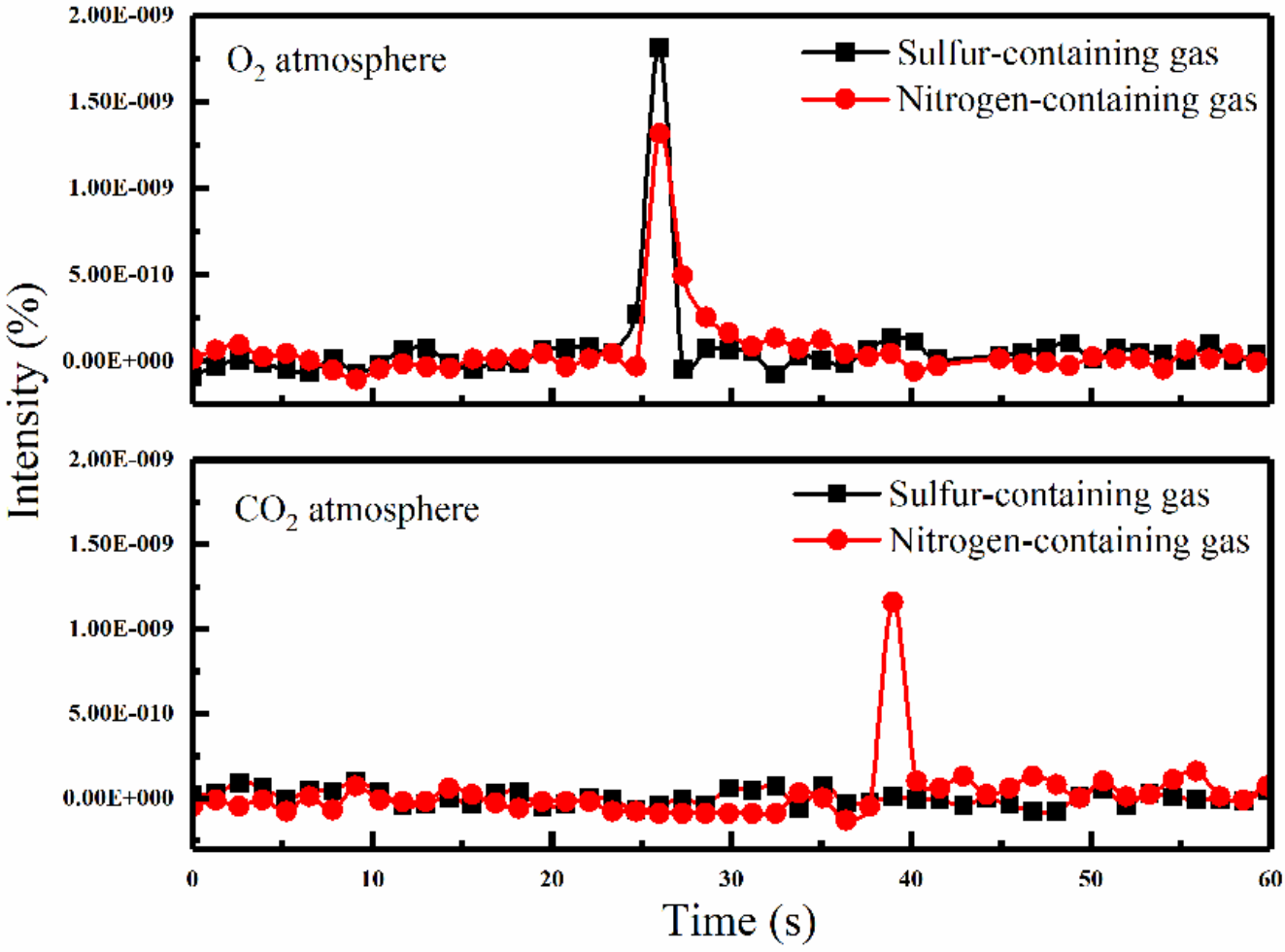

Figure 5

Gaseous pollutant production during hydrochar combustion and gasification.

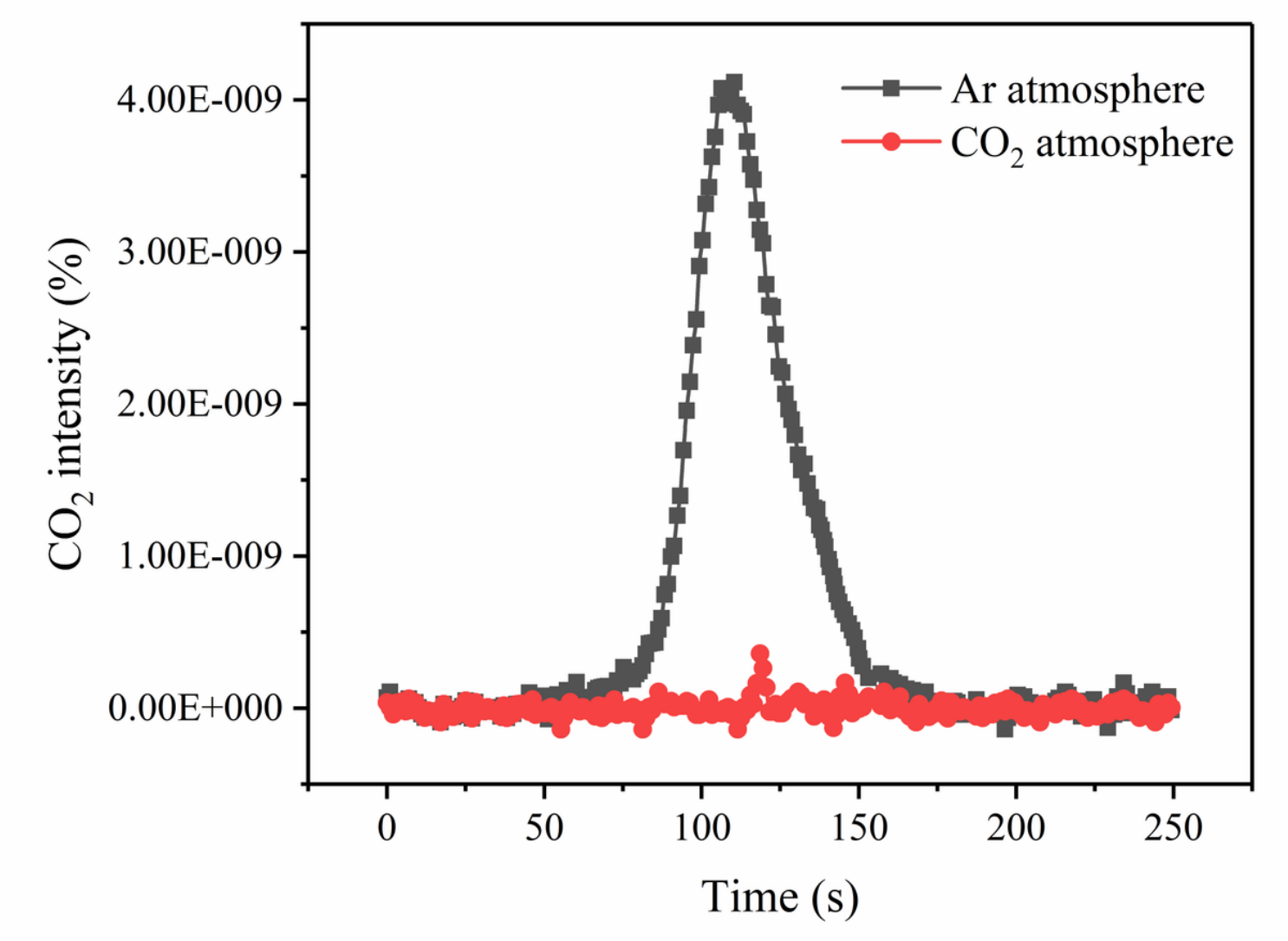

Figure 6

CO2 release during the combustion of residual char obtained after gasification in CO2 and Ar atmospheres.

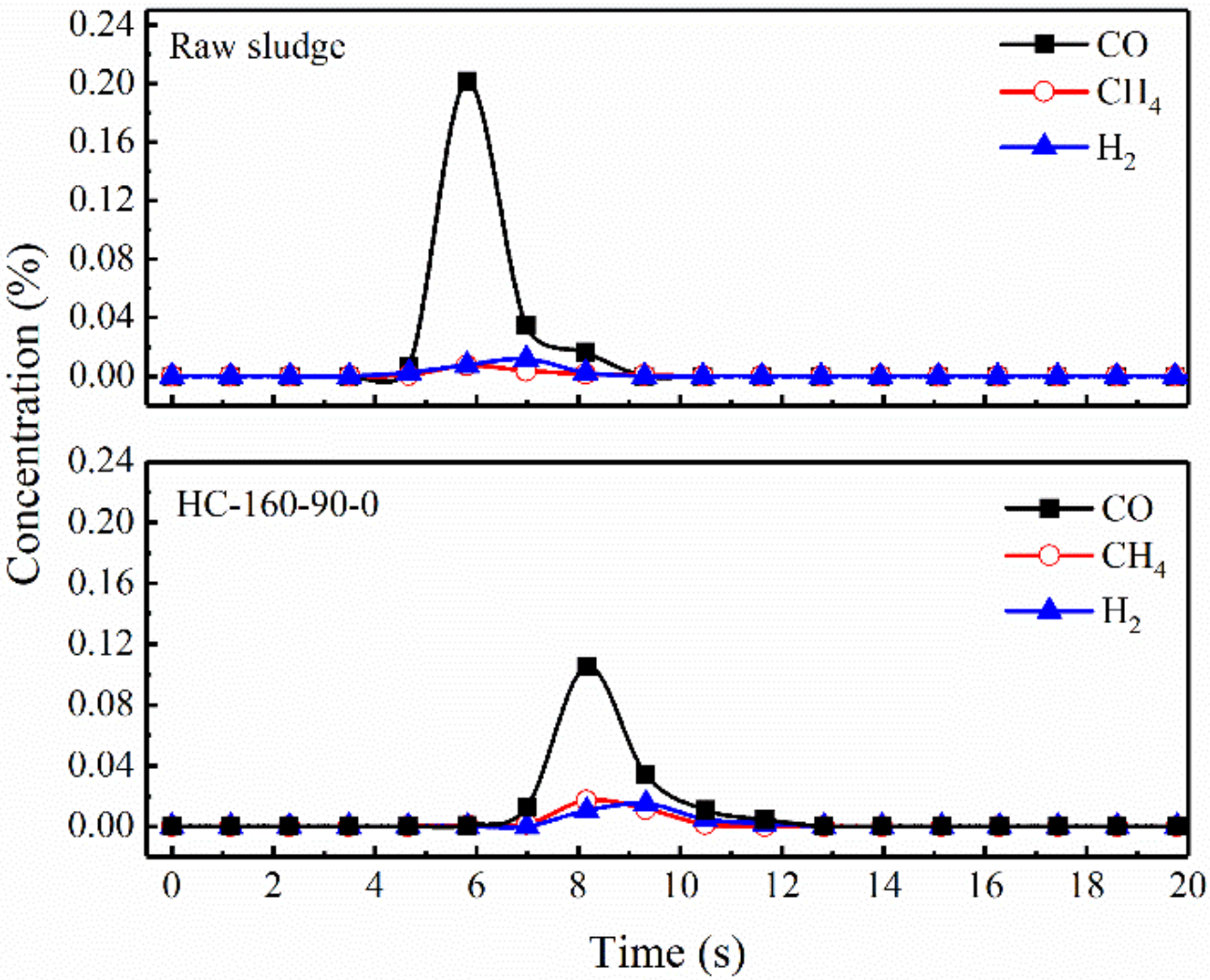

Figure 7

Evolution of gaseous products during the gasification of raw SS and sludge hydrochar.

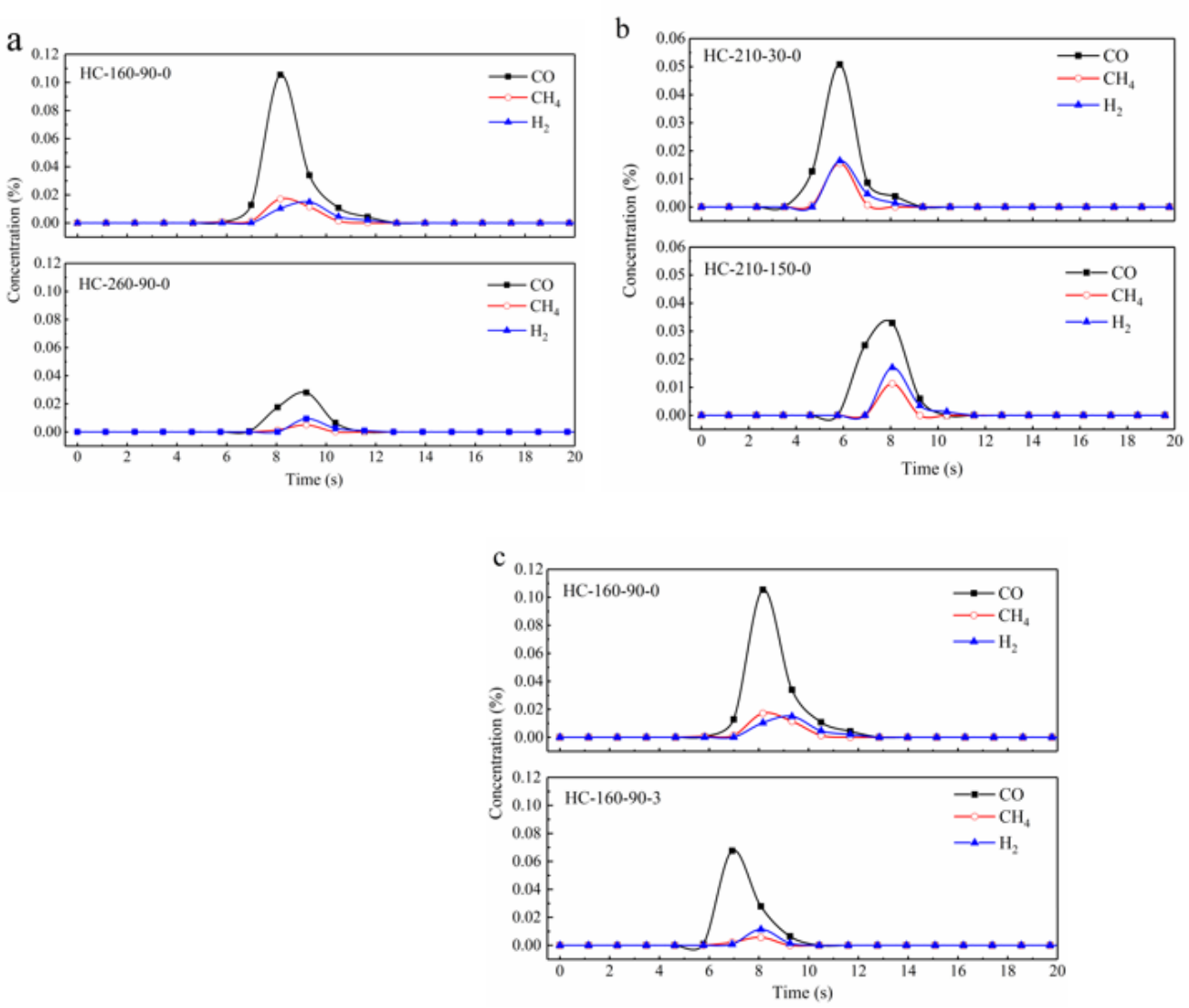

Figure 8

Effects of (a) temperature, (b) residence time, and (c) acetic acid concentration on the release of gaseous products during CO2-assisted gasification.

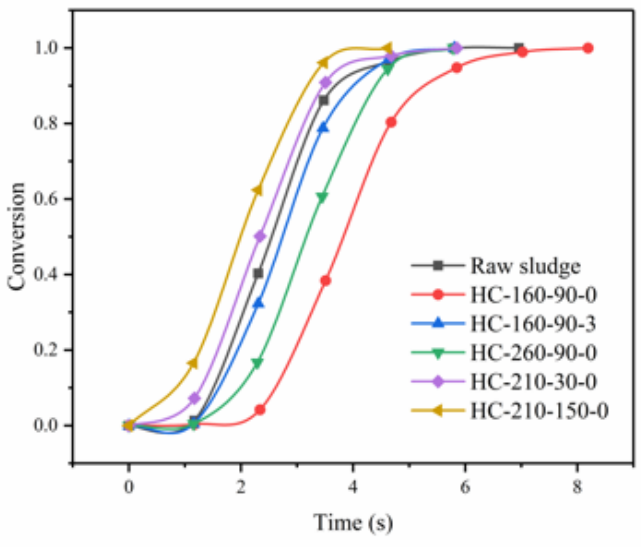

Figure 9

Effects of HTC conditions on the conversion of raw sludge and sludge hydrochar during gasification.

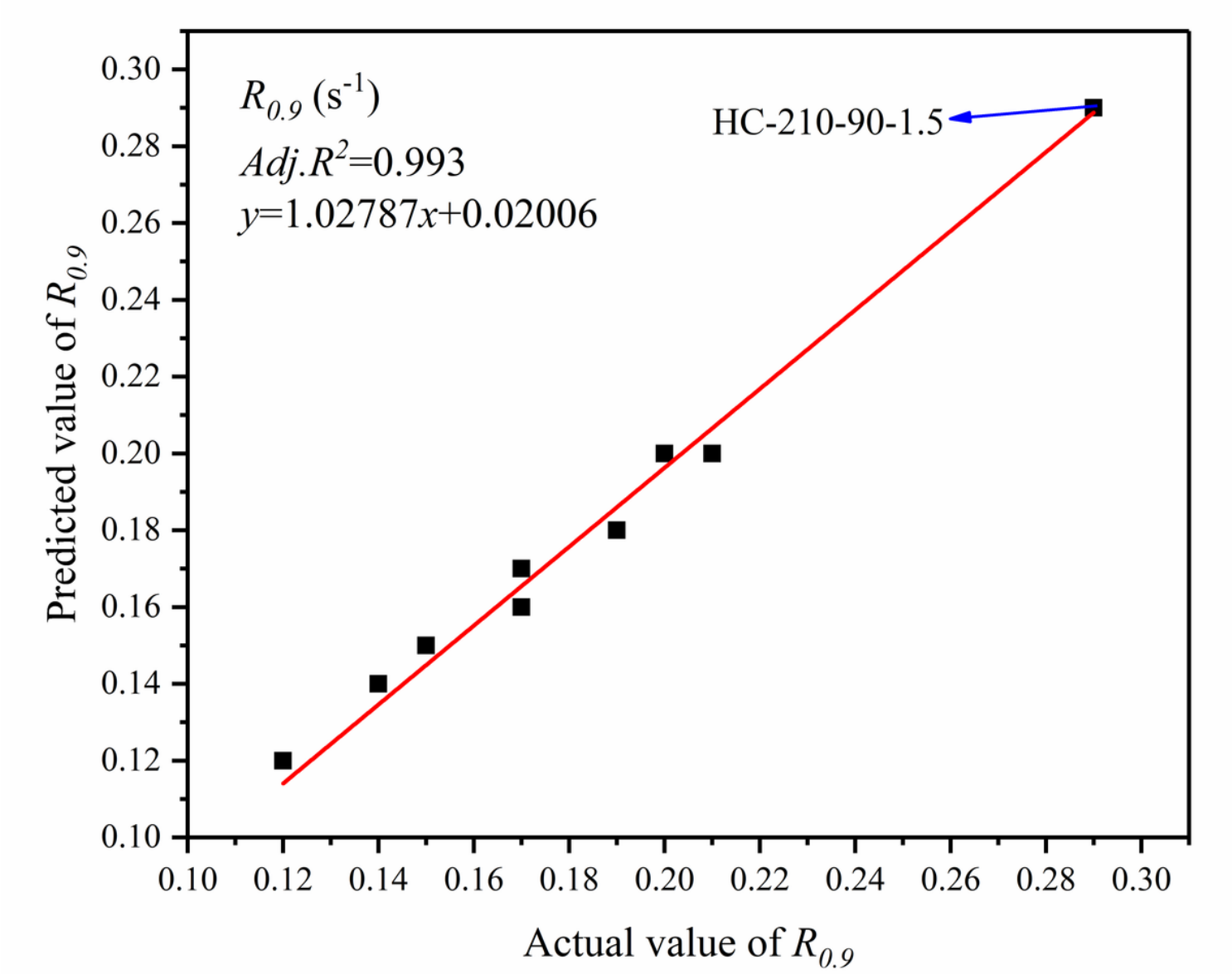

Figure 10

Comparison between actual and predicted indexes of gasification reactivity.

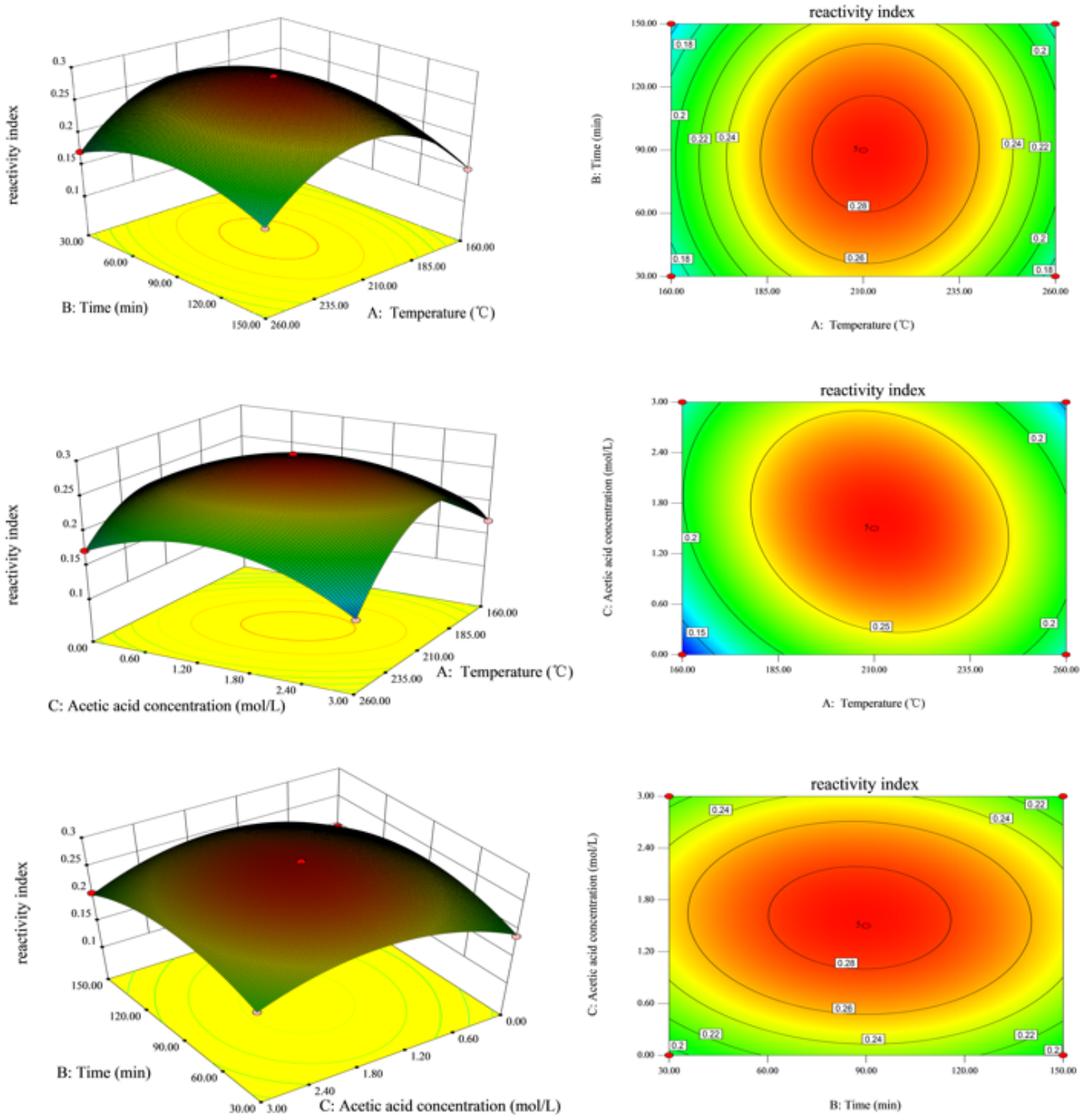

Figure 11

Response surface maps (a, c, e) and contour maps (b, d, f) showing the effects of temperature, residence time, and acetic acid concentration on the gasification activity index of hydrochar.